Proceedings of the
Annual Stability Conference
Structural Stability Research Council
Atlanta, Georgia, April 22-24, 2020

Seismic performance of double-skin composite walls with recycled aggregate concrete infill and corrugated faceplates

Qiuhong Zhao[1], Yikang Li[2], Ying Tian[3]

Abstract
An innovative composite wall, namely corrugated double-skin recycled aggregate concrete composite (Co-DR) wall, consisting of recycled aggregate concrete (RAC) filled steel tubes, two exterior steel faceplates connected by tie bolts with RAC infill, was proposed in this paper. Three double-skin composite wall specimens with different type of infilled concrete and faceplate profile were tested under combined axial and cyclic lateral loads. Failure mode, cyclic behavior, strength properties, deformation and energy dissipation capacities of the specimens were presented. Test results indicated that all specimens presented compression-flexure failure and showed expected seismic performance. Using RAC as infilled concrete decreased lateral strength and ductility of the double-skin composite wall slightly, while using corrugated plates as faceplates contributed to improve lateral strength, ductility, and energy dissipation capacity of the double-skin composite wall significantly. Comparing with the double-skin composite wall with flat faceplates and normal concrete, the double-skin composite wall with corrugated faceplates and recycled concrete presented competitive seismic performance, with a lateral strength increased by 10.92%, a ductility ratio decreased by 5.23%, and a cumulative energy dissipation increased by 16.51%. It is acceptable to use the double-skin composite wall with RAC as infilled concrete and corrugated plates as exterior faceplates as lateral load resisting system for mid- to high-rise buildings in seismic zones.

1. Introduction
Double-skin composite (DSC) wall consists of two exterior steel faceplates connected to each other by connectors and infilled with concrete. DSC wall was first proposed for coastal buildings to resist extreme loads (Stephens and Zimmerman 1990). Afterwards, more DSC walls were then proposed for use in tunnels and safety-related nuclear facilities, with different types of connectors such as headed studs (Shanmugam et al. 2002), Bi-Steel™ connectors (Mckinley and Boswell 2002; Clubley et al. 2003), and J-hook connectors (Liew and Sohel 2009; Huang and Liew 2016). Recently, DSC walls have also been used as a lateral-load resisting system in building structures, usually with concrete-filled steel tubes as the boundary elements and

[1] Professor, Tianjin University, <qzhao@tju.edu.cn>
[2] Ph.D. Candidate, Tianjin University, <liyikang@tju.edu.cn>
[3] Professor, University of Nevada, <ying.tian@unlv.edu>

faceplates connected by tie bolts (Ji et al. 2013; Rassouli et al. 2016) or batten plates (Nie et al. 2013). Research has proven that the DSC walls present high axial and lateral strengths, lateral stiffness, ductility, and energy dissipation capacity. Moreover, the use of steel faceplates improves construction efficiency because they function as stay-in-place formwork for concrete casting.

The faceplates of aforementioned DSC walls were usually flat. Related studies on flat DSC walls conducted by the authors showed that out-of-plane deformation of flat faceplates can be obviously observed after concrete casting. On the other hand, Bhardwaj and Varma (2016) pointed that the flat faceplates tend to develop imperfections during transportation and assembly. This imperfection would be amplified due to the pressure exerted by concrete pouring. Further, the amplified imperfection would decrease the axial strength of the DSC wall. Moreover, the ratio of connector spacing to flat faceplate thickness was suggested to be limited to 37 (Wright 1995) to ensure that local buckling does not occur before yielding. These might require the use of a large number of connectors, thereby leading to complex fabrications.

Wright and Gallocher (1995) proposed a type of DSC wall panel using cold-formed profiled steel sheeting as the exterior faceplates. The profiled steel sheeting had much higher out-of-plane bending stiffness than the flat faceplates, which was conducive to decrease the number of connectors. However, these composite panels were not constructed with any boundary column with an aim of resisting shear only. In fact, the use of boundary columns can significantly improve the deformation and energy dissipation capacity for DSC walls (Qian et al. 2012; Ji et al. 2013).

Recently in China, with the rapid development of construction industry, the natural resources, such as river sand and stone, is being deficient due to the rapid development of construction industry. Meanwhile, billion tons of construction waste is generated each year. The traditional disposal method of landfill or dumping had fatal impact on environment. Recycling and reuse of these construction waste become an inevitable choice. Using recycled aggregate concrete (RAC), which is partially replacing the natural aggregate in mix proportion by recycled aggregate, is a resolution considering both the shortage of natural resources and disposal of construction waste. However, research showed that the compressive strength of RAC was lower than that of normal concrete (NC) due to the relatively weak interfacial transition zone between the cement paste and the aggregates (Nixon 1978; Gerardu and Hendriks 1985; Hansen 1986; Mandal and Gupta 2002). Previous research also showed that the RAC shear walls had lower ductility than NC shear walls (Cui et al. 2012; Geng et al. 2016). This would decrease the seismic performance of the mid- to high-rise building structures.

This paper presents a new type of DSC shear wall system, namely corrugated double-skin recycled aggregate concrete composite (Co-DR) wall, to be used in mid- to high-rise buildings in seismic zones. The proposed Co-DR wall system consists of corrugated double steel faceplates connected by tie bolts, infilled RAC, and RAC-filled steel tube boundary columns. The corrugated steel plates and steel tubes are fabricated by hot-rolled steel to meet the ductility requirements of seismic design. Cyclic tests were carried out on three specimens with different type of infilled concrete (RAC or NC) and faceplate profile (flat or corrugated faceplate). The seismic performance of the test specimens was evaluated in terms of damage and failure pattern, hysteretic response, strength and stiffness characteristics, deformation property, and energy dissipation capacity.

2. Experimental Program

2.1 Specimen Design

Three specimens, denoted as CW-F, RCW-F, and RCW-C, were fabricated at 1/3 scale to accommodate the capacity of the loading facility and the Chinese provision JGJ/T 101-2015 (CMC 2015). The source of the recycled coarse aggregate (RCA) used in this test was derived from the demolition of a building in Beijing. It was produced through a series of processes such as crushing, sieving, cleaning and many other processes in a recycled aggregate plant. The RCA replacement percentage was defined as the percentage of the RCA mass to the total coarse aggregates mass. Specimen CW-F was a double-skin composite shear wall with flat steel plates and NC. Specimen RCW-F was a double-skin composite shear wall with flat steel plates and RAC with RCA replacement percentage of 100%. Specimen RCW-C was a double-skin composite shear wall with corrugated steel plates and RAC with RCA replacement rate of 100%. The two parameters studied in this experiment were the infilled concrete (NC or RAC) and the faceplate type (flat or corrugated faceplate). According to the relevant Chinese code for seismic design of buildings (CMC 2010a), two square concrete filled steel tube (CFT) columns were employed as boundary elements. For these three specimens, the extent of a square CFT column was designated to be 0.15 times the wall cross-sectional depth. The size of a square CFT column was 150 × 150 mm. Two exterior faceplates were fastened by high strength bolts with a diameter of 8 mm (D8). The transverse spacing of tie bolts was 140 mm and the vertical spacing of tie bolts was 150 mm. A loading beam and a foundation beam in the form of exterior faceplates with infilled concrete were welded and cast together with the wall. The square CFT columns and faceplates were embedded to the loading beam and the foundation beam. Anchor bars and headed studs were installed to ensure sufficient anchorage strength. For three specimens, the distance from the horizontal load point to the top of the foundation beam was all 1500 mm, leading to an aspect ratio of 1.5. Details of specimens are summarized in Table 1. Fig. 1(a) and (c) show the overall geometry, structural layout, and details of Specimens CW-F and RCW-F. Two specimens were identical, except for the infilled concrete. Fig. 1 shows the overall geometry, structural layout, and details of the specimens.

Table 1. Details of specimens.

Specimen number	Height (mm)	aspect ratio	Tie bolts spacing (mm)	RCA replacement percentage (%)	faceplate profile
CW-F	1500	1.5	140 × 150	0	Flat
RCW-F	1500	1.5	140 × 150	100	Flat
RCW-C	1500	1.5	140 × 150	100	Corrugated

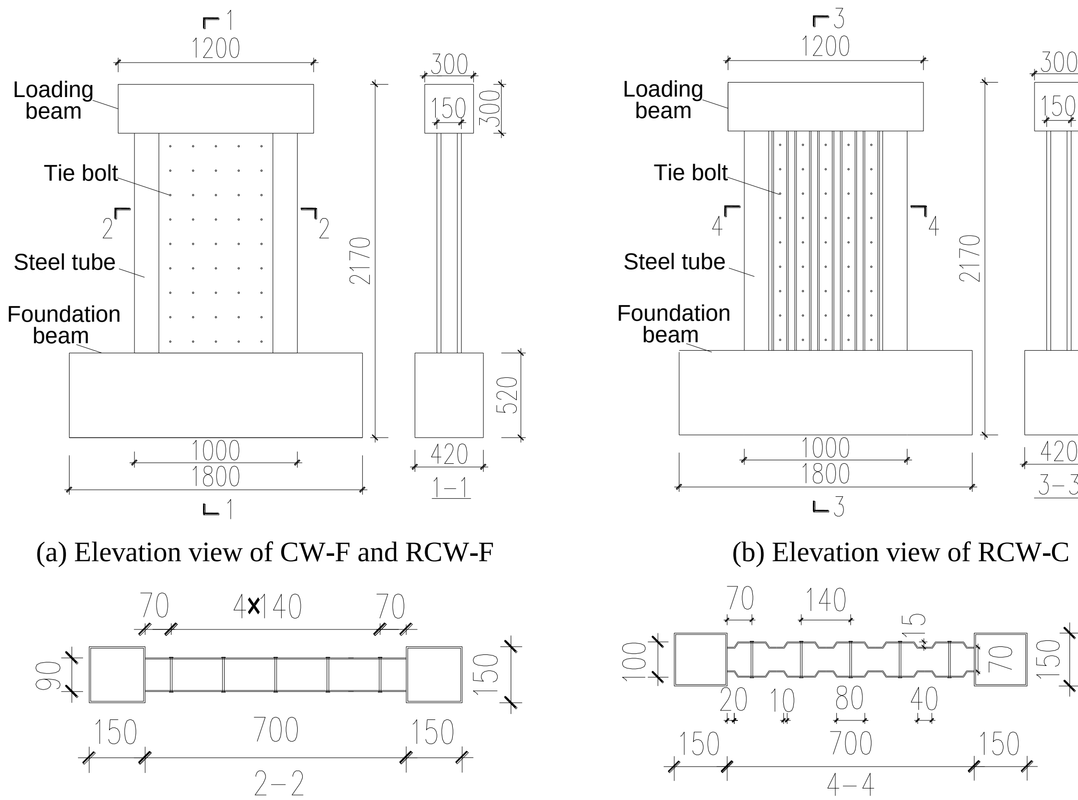

(a) Elevation view of CW-F and RCW-F

(b) Elevation view of RCW-C

(c) Section 2-2 of CW-F and RCW-F

(d) Section 4-4 of RCW-C

Figure 1: Dimensions and details of specimens (unit: mm)

2.2 Material Properties

The RCA was continuous graded gravels. The particle size of RCA was 5-25 mm. The apparent density of RCA was 2543 kg/m^3 and other results were summarized in Table 2. The test results shown that the RCA could meet the requirements in the GB/T 25177-2010 (CMC 2010b) for crushed stone.

Table 2. Basic properties of recycled coarse aggregate.

Type	Grading (mm)	Water absorption (%)	Index of crushing (%)	Elongated or flat particle (%)
RCA	5-25	4.3	12	2.7

The fine aggregate used was river sand with continuous graded gravels and a fineness modulus of 2.3. The natural coarse aggregate (NCA) was also continuous graded gravels. The particle size of NCA was 5-25 mm. Ordinary Portland cement with a 28^d compressive strength of 42.5 MPa was used in this test. The mix design of RAC was in accordance with the JGJ 55-2011 (CMC 2011). The NC of grade C40 was taken as datum concrete. The RCA replacement percentage was 0% and 100% in this test. Considering the characteristic of higher water absorption capacity of RCA, the method of "pre-absorbing water" proposed by Zhang et al. (2002) was adopted in order to improve workability and mechanical properties of the RAC. Divided the amount of water used in the mix proportions of RAC into two parts, one part was the conventional water amount from the mix design, and the other part was the additional water amount after considering the higher water absorption capacity of RCA. The additional water amount was determined according to ten minutes-water absorption capacity of RCA. Through the water absorption test, it was founded that the water absorption was 2.19% in ten minutes. For the convenience of test, two parts of water amount were added simultaneously during concrete mixing. The mix proportions of concrete under different RCA replacement percentages are listed in Table 3. Three 100 mm cube samples were cast along with each specimen. Concrete compressive tests were conducted on the day of specimen testing. The cylinder compressive strength was obtained as 33.9, 31.6, and 31.6 MPa for Specimens CW-F, RCW-F, and RCW-C, respectively.

Table 3. Mix proportions of concrete.

Type	RCA replacement percentage (%)	Mix proportions (kg/m^3)				
		Cement	Sand	NCA	RCA	Water
NC	0	380	710	1080	0	184
RAC	100	380	710	0	1080	208

Tensile tests were conducted on coupons cut from the steel components used for the specimens. Table 4 gives the measured yield strength, ultimate tensile strength, Young's modulus, and yield strain of the steel materials. The high strength tie bolts had a nominal yield stress of 640 MPa and ultimate strength of 800 MPa.

Table 4. Material properties of steel.

Steel type	Nominal thickness (mm)	Measured thickness (mm)	Yield strength f_y (MPa)	Tensile strength f_u (MPa)	Young's modulus E_s (MPa)
Faceplate	3	2.60	307	445	2.0×10^5
Tube	4	3.45	314	388	1.9×10^5

2.3 Test setup and Loading Protocol

Fig. 2 shows the test setup for applying axial and lateral loads. The foundation beam was fixed to a strong floor by two steel beams and fastening rods, and clamped by a pair of reaction block on each side of the specimen to restrain its horizontal movement. Axial load was applied by a vertical jack. A rolling support between the vertical jack and the loading beam was provided to accommodate the horizontal movement of the specimen due to lateral displacements. A steel spreader beam was used to distribute the axial load evenly to the specimen. Horizontal cyclic loading was applied at the mid-height of the loading beam by a hydraulic actuator fixed to a reaction wall. Both the horizontal actuator and the vertical jack had a loading capacity of 2000 kN.

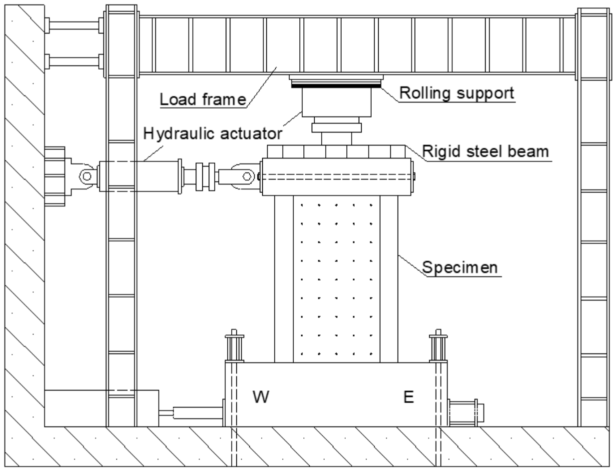

Figure 2: Test setup

The axial load was determined by an axial load ratio of n = 0.2, which was calculated by Eq. (1), and maintained constant during the test.

$$n = \frac{N}{f_c' A_c + f_{yp} A_p + 2 f_{yt} A_{ts}} \tag{1}$$

where A_c = cross area of wall concrete; f_{yp} = yield strength of steel faceplates; A_p = total cross area of two steel faceplates; f_{yt} = yield strength of steel tubes; and A_{ts} = cross area of a single steel tube.

The lateral cyclic loading was applied by the horizontal hydraulic actuator quasi-statically. Fig. 3 shows the loading history in terms of drift ratio, defined as the ratio of horizontal displacement at the loading beam to wall effective height, and the loading cycle number at each drift level. The initial loading contained drift ratios of 0.125, 0.25, and 0.375% with one loading cycle per drift level. The following loading contained drift ratios of 0.5, 0.75, 1, 1.5, 2, 2.5, and 3% drifts with two loading cycles at each drift ratio.

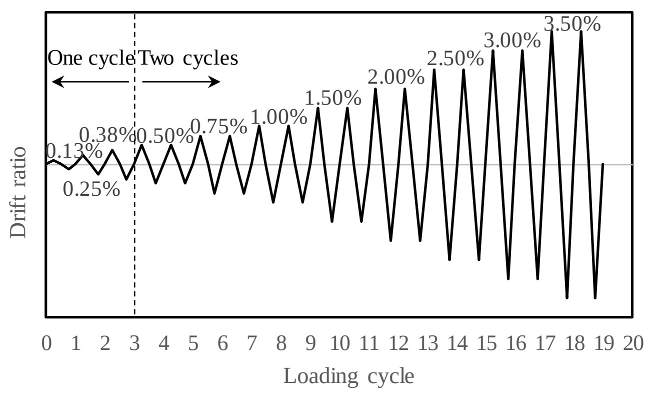

Figure 3: Lateral loading procedure

2.4 Instrumentation

Instruments were used to measure forces, displacements and strains in the specimen during the testing. The vertical and lateral loads were measured by load cells. Linear variable differential transformers (LVDTs) were used to measure the lateral displacement, vertical displacement and shear displacement. The layout of LVDTs, which were installed at Specimen RAC-C, were shown in Fig. 4(a). For Specimens CW-F and RAC-F, the layout of LVDTs was the same as that of Specimen RAC-C. A range of LVDTs (i.e., L1-L6) measured the flexural deformation of the composite shear wall. L6 was used to monitor horizontal slip of the foundation beam. A pairs of crossed LVDTs (i.e., B1 and B2) measured the shear deformation of the composite shear wall. Two LVDTs (i.e., V1 and V2) were used to monitor the rotation of the foundation beam. Two LVDTs (i.e., V3 and V4) were mounted to the specimen at the same height as LVDT L2, measuring the vertical displacement of the composite shear wall. Strain gauges and strain rosettes were attached to the steel tubes and steel faceplates to measure their longitudinal strains and strains in three directions. Fig. 4(b) shows an example of the arrangement of strain gauges and strain rosettes, which was the same for all test specimens.

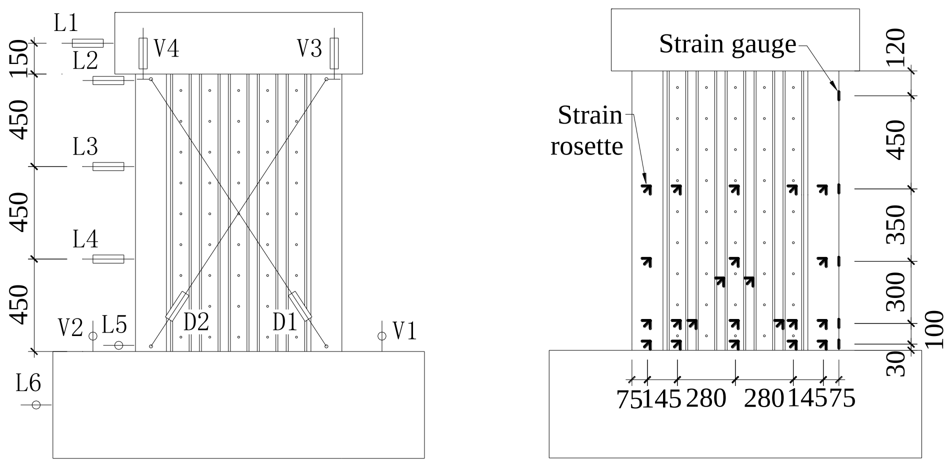

(a) LVDTs and dial gauges (b) Strain gauges and strain rosettes

Figure 4: Instrumentation for Specimen RAC-C (unit: mm)

3. Test Results

3.1 General Behavior

3.1.1 Elastic Stage

At the initial stage of test, the cooperative work performance of steel plates, steel tubes and the infilled concrete was good. The whole specimen was intact and there was no obvious phenomenon. Occasionally there was the slight sound of concrete crushing, indicating local adhesive destruction at the interface between steel plates and infilled concrete. There was a slight separation at the interface between the bottom of steel tubes and the foundation beam. The lateral load displacement relation curves of three specimens were basically linear, and the residual deformation was negligible.

3.1.2 Damage Developing Stage

This stage started from the lateral load-displacement hysteresis loop of the specimen shown a significant turning point to the point of peak load point of the specimen. The main experimental phenomena of three specimens in this stage was the further development of the local adhesive destruction at the interface between steel plates and infilled concrete, and the local buckling at the bottom of steel tubes and steel plates. As the amplitude of displacement increased, the extent of local buckling increased continuously. The obvious local buckling occurred at the bottom of steel tubes of three specimens, and the steel plates at the bottom of wall web experienced local buckling, as shown in Fig. 5, when the drift ratio increased to 1% drift.

For Specimens CW-F and RCW-F, a slight residual buckling occurred at the bottom of steel tubes, and the buckling of the steel plates at the bottom of wall web was increased continuously, when the drift ratio increased to 1.5%. For Specimen RCW-C, local buckling occurred at the crest of the bottom of steel plates, and a slight residual buckling occurred at the bottom of steel tubes at 1.5% drift. For Specimen RCW-C, when the drift ratio increased to 1.5%, a new buckling located in the bottom of steel tubes occurred, and local buckling occurred at the crest and trough of the bottom of wall.

At this stage, the stiffness of the specimen was gradually reduced, and the lateral load displacement hysteresis loop of the specimen shown obvious nonlinear characteristics. No obvious buckling in the middle and upper part of the steel plates at wall web occurred at three specimens.

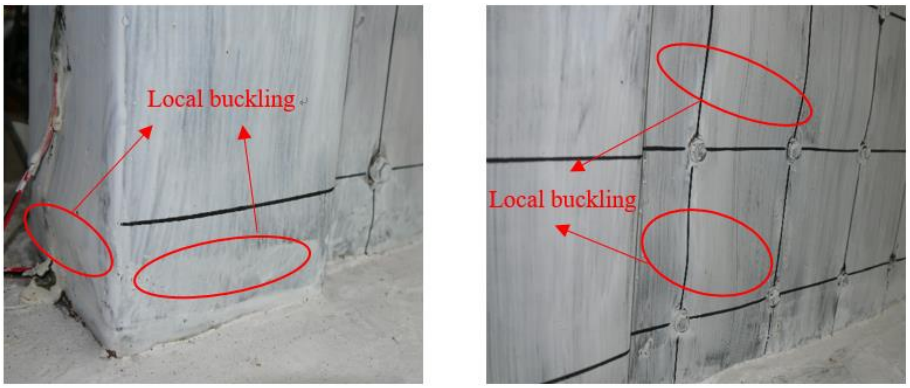

(a) CW-F (b) RCW-F

Figure 5: Specimens CW-F and RCW-F at damage developing stage

3.1.3 Failure Stage

After specimen reached the peak load, the infilled concrete damage was aggravated with the increased drift ratio. The local buckling was severely increased at the base of steel tubes, as well as the residual deformation. For Specimens CW-F and RCW-F, when the drift ratio finally increased to 2.5%, the steel tube occurred tensile fracture along the horizontal direction. Then infilled concrete crushing was observed immediately. The buckling at the bottom of the steel plates at the bottom of wall web was increased severely, and extended towards the middle of the shear wall. Therefore, the specimens lost their vertical load-carrying capacity and the tests were terminated. For Specimen RCW-C, when the drift ratio increased to 2.5%, the steel tube occurred tensile fracture along the horizontal direction, as shown in Fig. 6. Afterwards, when the drift ratio finally increased to 3%, the tensile fracture was aggravated and the specimen lost its vertical load-carrying capacity and the test was terminated. Failure patterns of the specimens after loading are shown in Fig. 7.

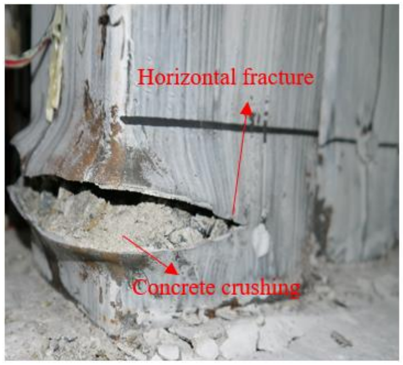

Figure 6: Tube failure of Specimen RCW-C at 2.5% drift

Figure 7: Failure patterns of the test specimens after loading

3.2 Lateral Load-Displacement Relationship

Hysteretic loops can reflect important information such as strength, stiffness, failure mechanism and energy dissipation capacity of specimens. In addition, it can comprehensively reflect their seismic performance. The hysteresis loops of lateral load-displacement relationship of Specimens CW-F, RCW-F and RCW-C are shown in Fig. 8. The hysteresis loops of three specimens were shuttle shaped and full, which indicated that these composite shear walls had good energy dissipation capacity and superior seismic performance. According to the behavior of the specimens, the loading process could be categorized into three stages, namely elastic stage, elastic-plastic stage and failure stage. During the elastic stage, the hysteresis loops of the specimens were approximately a straight line, and the residual deformation was small. Besides, strength and stiffness were not degraded. During the elastic-plastic stage, as the lateral displacement increased, cracks appeared in the infilled concrete, and slight local buckling occurred at the bottom of the steel tubes and the wall plates. Besides, the strength of the specimens increased gradually, and the strength began to deteriorate. However, the degree of deterioration was relatively small. The stiffness of the specimens began to gradually reduce due to the phenomenon of stiffness degradation. The hysteresis loops were relatively full, and the area of the hysteresis loop began to increase significantly. In addition, the residual deformation increased with the increase of the horizontal displacement after unloading. During the failure stage, after the horizontal load had passed the peak load, the infilled concrete damage was aggravated, and the local buckling at the bottom of the steel tubes and the wall plates were serious. Besides, the strength of the specimens was reduced more obviously. The strength degradation phenomenon was significant. The stiffness of specimens became larger and the stiffness degradation phenomenon was significant. The shape of the hysteresis loops was still full and the residual distortion increased sharply.

Fig. 9 shows the envelope curves of three specimens. The envelope curves of the lateral force versus displacement relationships were inverted "S" shape, indicating the force process of the three specimens was similar and it could be divided into elastic stage, elastic-plastic stage and failure stage. Furthermore, the envelope curves of the three specimens were relatively smooth, indicating that the change in lateral strength and stiffness of all specimens was smooth and the ductility was good.

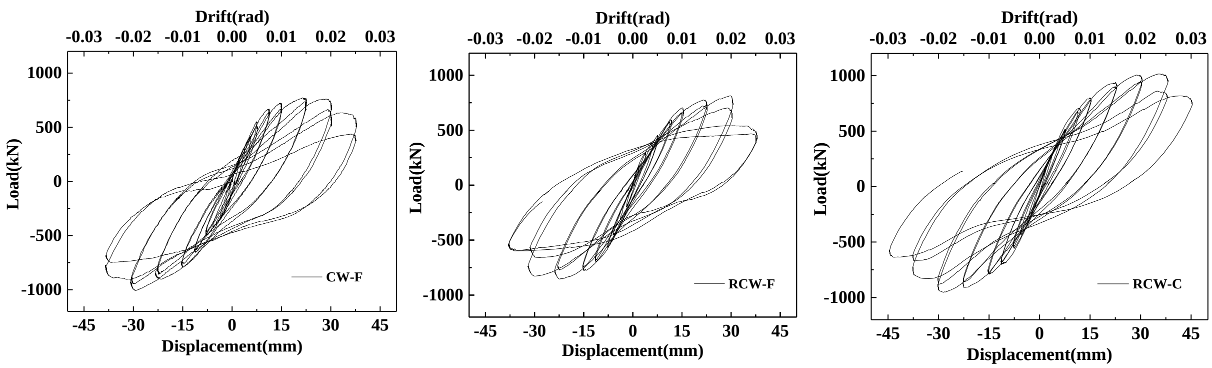

Figure 8: Hysteretic lateral load-drift responses

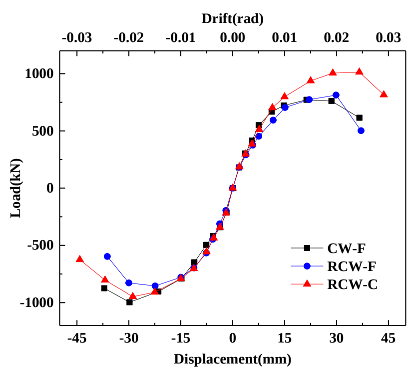

Figure 9: Envelope curves

3.3 Lateral Strength

The yield load P_y and yield displacement Δ_y were determined by using the method proposed by Han (2016). The load was defined as the ultimate load P_u when the lateral load decreased to 85% of the peak load P_m or the axial load could not be maintained and the specimen was deemed to fail completely. The displacement corresponding to the ultimate load P_u was the ultimate displacement Δ_u. The yield load P_y, yield displacement Δ_y, ultimate load P_u and ultimate displacement Δ_u of three specimens are shown in Table 5. The peak load of Specimen RCW-F was reduced by 5.71% compared with Specimen CW-F, indicating that the use of RAC in composite shear walls would reduce their lateral strength. While the peak load of Specimen RCW-C was 17.64% higher than Specimen RCW-F, indicating that the use of corrugated steel plates in the composite shear walls would noticeably increase their lateral strength and promote seismic performance. For corrugated steel plates, they have lots of corrugated edges. Therefore, when compared with flat steel plates, the stiffness of corrugated steel plates is greater; the time of buckling is later; the degree of buckling is lighter; the constraint effect on the infilled concrete is stronger, and the cooperative work of the corrugated steel plates and the infilled concrete is better. Besides the peak load of Specimen RCW-C was 10.92% higher than Specimen CW-F, indicating that the use of corrugated steel plates and RAC simultaneously in the composite shear wall would improve lateral strength.

Table 5. Results of main stages.

Specimen	Force direction	Yield stage		Peak stage		Ultimate stage		u
		P_y / kN	Δ_y / mm	P_m / kN	Δ_m / mm	P_u / kN	Δ_u / mm	
CW-F	Push	559	7.8	771	21.3	655	34.4	4.39
	Pull	526	8.3	997	29.8	874	36.6	4.40
RCW-F	Push	484	8.4	813	29.9	691	32.7	3.88
	Pull	601	8.6	854	22.4	726	32.7	3.83
RCW-C	Push	655	10.5	1013	36.6	861	42.0	3.99
	Pull	586	8.3	948	28.9	806	36.0	4.34

3.4 Deformation Capacity

Ductility, defined as the ratio of ultimate displacement to yield displacement, was used to measure the deformation capacity of the specimens. The ductility ratio of each specimen is shown in Table 5. The ratios of the average yield displacement to the height of specimens, the ratios of average peak displacement to the height of specimens and the ratios of average ultimate displacement to the height of specimens were defined as the yield drift ratio θ_y, the peak drift ratio θ_m and the ultimate drift ratio θ_u, respectively. The calculation results are shown in Table 6. Table 5 and 6 indicate the following observations. (1) For three specimens, the yield drift ratio was between 0.54 to 0.63%, the ultimate drift ratio was between 2.18 to 2.60%, and the ratio of the ultimate drift ratio to the yield drift ratio was above 3, indicating that specimens had good deformation capacity, and there were obvious signs before the failure. (2) The displacement ductility ratio of the three specimens was between 3.83 and 4.40, indicating the ductility of double-skin recycled concrete filled composite shear walls was good. (3) The displacement ductility ratio of Specimen RCW-F was 12.29% lower than Specimen CW-F, indicating that the use of RAC in the composite shear wall would reduce their ductility. The main reason was that the deformation capacity of RAC was worse than that of NC. (4) The displacement ductility ratio of Specimen RCW-C was 8.04% higher than Specimen RCW-F, indicating that corrugated steel plates had significant influence on the displacement ductility of the wall. Using corrugated steel plates in DSC walls can improve displacement ductility ratio observably. (5) The displacement ductility ratio of Specimen RCW-C was 5.23% lower than Specimen CW-F, indicating that compared with double-skin composite shear wall with flat steel plates and NC, when RAC and corrugated steel plates were used in composite walls simultaneously, the reduction of the displacement ductility ratio was slight.

Table 6. Drift ratio of main stages.

Specimen	Drift ratio		
	θ_y / %	θ_m / %	θ_u / %
CW-F	0.54	1.71	2.37
RCW-F	0.57	1.74	2.18
RCW-C	0.63	2.18	2.60

3.5 Energy Dissipation

Based on the lateral force displacement hysteresis loops of specimens and calculated the energy dissipation each half cycles by the integral, the energy dissipation capacity of the specimen in the whole loading process could be evaluated comprehensively. The half cycle energy dissipation versus number of half cycles and the cumulative energy dissipation versus number of half cycles of the specimens are shown in Fig. 10. The half cycle energy dissipation and cumulative energy dissipation of three specimens increased with the increase of half cycle number. In the elastic stage, the energy dissipation of the specimens increased slowly, and after entering the elastic-plastic stage, the energy dissipation of the specimens increased rapidly. It was shown that the energy dissipation capacity of the specimen was increased rapidly after entering the elastic-plastic stage, and the energy dissipation capacity was good. The cracking of infilled concrete was delayed by the constraint of two outer steel plates. Besides, the half cycle energy dissipation and cumulative energy dissipation of the Specimen RCW-F was similar to those of the Specimen CW-F, and the half cycle energy dissipation was reduced by 0.11%. It was shown that the energy dissipation capacity of RAC used in this kind of composite shear wall was reduced slightly, and the energy dissipation capacity was good. While the half cycle energy dissipation and cumulative energy dissipation of the Specimen RCW-C were similar to those of the Specimen RCW-F, and the half cycle energy dissipation was increased by 16.64%. It was shown that corrugated steel plates were more helpful for improving the energy dissipation capacity of composite shear walls. The cooperative work between corrugated steel plates and infilled concrete was better, therefore, the Specimen RCW-C had higher energy dissipation capacity. In addition, the half cycle energy dissipation and cumulative energy dissipation of the Specimen RCW-C were similar to those of the Specimen CW-F, and the half cycle energy dissipation was increased by 16.51%. It was shown that the energy dissipation capacity of Specimen RCW-C was better. The use of RAC for double-skin corrugated steel plates composite shear walls provided good seismic performance.

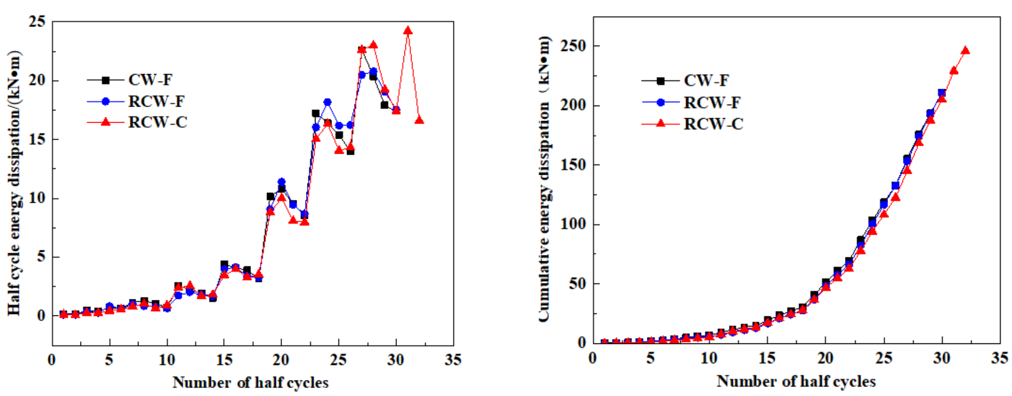

(a) Energy dissipation per half cycle (b) Cumulative energy dissipation

Figure 10: Energy dissipation capacities

4. Conclusions

This paper proposed an innovative composite wall, namely corrugated double-skin recycled aggregate concrete composite (Co-DR) wall. To investigate the cyclic behavior of the walls, a series of quasi-static tests of three specimens were conducted. The failure modes and seismic performance of the composite walls are summarized as follows:

(1) The composite walls failed in the sequence of the local buckling at the base of steel tubes, the local buckling of steel plates at the bottom of the wall, the fracture of steel tubes, and compressive crushing of concrete at the bottom of the wall. Three specimens presented a flexural failure mode.

(2) This composite shear wall presented a good strength capacity, ductility, deformation, energy dissipation capacity, which indicated this composite shear wall had an excellent seismic performance.

(3) Compared with double-skin composite shear wall with flat steel plates and NC, the peak load, the ductility and the cumulative energy dissipation of double-skin composite shear wall with flat steel plates and RAC were slightly reduced. The peak load was reduced by 5.71%, the displacement ductility factor was reduced by 12.29%, and the cumulative energy dissipation was reduced by 0.11%, indicating that it was feasible to use RAC in composite shear walls.

(4) Compared with double-skin composite shear wall with flat steel plates and RAC, the peak load, the ductility and the cumulative energy dissipation of double-skin composite shear wall with corrugated steel plates and RAC were obviously improved. The peak load was increased by 17.64%, the displacement ductility factor was increased by 8.04%, and the cumulative energy dissipation was increased by 16.64%, indicating that the cooperative work between corrugated steel plates and infilled RAC was better and corrugated steel plates could significantly improve the seismic performance.

(5) Compared with double-skin composite shear wall with flat steel plates and NC, the peak load and the cumulative energy dissipation of double-skin composite shear wall with corrugated steel plates and RAC were obviously improved. The peak load was increased by 10.92%, the displacement ductility factor was reduced by 5.23%, and the cumulative energy dissipation was increased by 16.51%, indicating that the use of corrugated steel plates and RAC in composite shear walls had significantly improved seismic performance and double-skin composite shear wall with corrugated steel plates and RAC was feasible in practical engineering.

Acknowledgments

The presented work was sponsored by the National Natural Science Foundation of China (Grants Nos. 51378340, 51678406 and 51878447). The authors would like to express their sincere gratitude to the sponsors.

References

Bhardwaj, S. R., Varma, A. H. (2016). “Effect of imperfections on the compression behavior of SC walls.” *Proc., Annu. Stabil. Conf. (SSRC 2016)*. Struct. Stabil. Res. Council, Orlando, FL.

Clubley S.K., Moy S.S.J., and Xiao R.Y. (2003). “Shear strength of steel-concrete-steel composite panels. Part I-testing and numerical modelling.” *Journal of Constructional Steel Research*, 59, 781-794.
CMC (China Ministry of Construction). (2010a). “Code for seismic design of buildings.” *GB 50011-2010*, Beijing (in Chinese).
CMC (China Ministry of Construction). (2010b). “Recycled coarse aggregate for concrete.” *GB/T 25177-2010*, Beijing (in Chinese).
CMC (China Ministry of Construction). (2011). “Specification for mix proportion design of ordinary concrete.” *JGJ 55-2011*, Beijing (in Chinese).
CMC (China Ministry of Construction). (2015). “Specification for seismic test of buildings.” *JGJ/T 101-2015*, Beijing (in Chinese).
Cui Z., Lu S., and Wang Z. (2012). “Feasibility experimental research on the application of shear wall with recycled aggregate concrete.” *Bulletin of the Chinese Ceramic Society*, 31(3), 716-719.
Geng Y., Wang Y., and Chen J. (2016). “Creep behaviour of concrete using recycled coarse aggregates obtained from source concrete with different strengths.” *Construction and Building Materials*, 128, 199-213.
Gerardu J.J.A., Hendriks C.F. (1985). “Recycling of road pavement materials in the Netherlands.” *Rijkswaterstaat Communications*, 1985(38).
Han L. (2016). *Concrete filled steel tubular structures-theory and practice*, Science Press, Beijing.
Hansen T.C. (1986). “Recycled aggregate and recycled aggregate concrete-second state of art report, development from 1945-1985.” RILEM Technical Committee 37 DR-C. *Material and Structures*, 19(5), 201-246.
Huang Z., and Liew J.Y.R. (2016). “Structural behaviour of steel-concrete-steel sandwich composite wall subjected to compression and end moment.” *Thin-Walled Structures*, 98, 592-606.
Ji X., Jiang F., and Qian J. (2013). “Seismic behavior of steel tube-double steel plate-concrete composite walls: Experimental tests.” *Journal of Constructional Steel Research*, 86, 17-30.
Liew J.Y.R., and Sohel K.M.A. (2009). “Lightweight steel-concrete-steel sandwich system with J-hook connectors.” *Engineering Structures*, 31, 1166-1178.
Mandal S., Gupta A. (2002). “Strength and durability of recycled aggregate concrete.” *IABSE Symposium Melbourne*, Melbourne, Australia.
Mckinley B., and Boswell L.F. (2002). “Behavior of double skin composite construction.” *Journal of Constructional Steel Research*, 58, 1347-1359.
Nie J., Hu H., Fan J., Tao M., Li S., and Liu F. (2013). “Experimental study on seismic behavior of high-strength concrete-filled double-steel-plate composite walls.” *Journal of Constructional Steel Research*, 88(9), 206-219.
Nixon P.J. (1978). “Recycled concrete as an aggregate for concrete-a review.” *Matériaux Et Construction*, 11(5), 371.
Qian J., Jiang Z., and Jiang F. (2012). “Behavior of steel tube-reinforced concrete composite walls subjected to high axial force and cyclic loading.” *Engineering Structures*, 36, 173-184.
Rassouli B., Shafaei S., Ayazi A., and Farahbod F. (2016). “Experimental and numerical study on steel-concrete composite shear wall using light-weight concrete.” *Journal of Constructional Steel Research*, 126, 117-128.
Shanmugam N.E., Kumar G., and Thevendran V. (2002). “Finite element modelling of double skin composite slabs.” *Finite Elements in Analysis and Design*, 38, 579-599.
Stephens M.J., and Zimmerman T.J.E. (1990). “The strength of composite ice-resisting walls subjected to combined loads.” *Proceedings of 1st European Offshore Mechanics Symposium (EUROMS-90)*, Golden, Colo.
Wright H.D. (1995). “Local stability of filled and encased steel sections.” *Journal of Structural Engineering*, 121(10), 1382-1388.
Wright H.D., and Gallocher S.C. (1995). “The behavior of composite walling under construction and service loading.” *Journal of Constructional Steel Research*, 35(3), 257-273.
Zhang Y., Qin H., Sun W., Hao D., and Ning Z. (2002). “Research on mix portion design of recycled aggregate concrete.” *China Concrete and Cement Products*, 1, 7-9. (in Chinese).